J. Cent. South Univ. (2020) 27: 1484−1494
DOI: https://doi.org/10.1007/s11771-020-4384-0

Springer

Growth of metallic iron particles during reductive roasting of boron-bearing magnetite concentrate

ZHANG Xin(张鑫), LI Guang-hui(李光辉), RAO Ming-jun(饶明军), MI Huan-peng(米寰鹏), LIANG Bin-jun(梁斌珺), YOU Jin-xiang(游锦香), PENG Zhi-wei(彭志伟), JIANG Tao(姜涛)

School of Minerals Processing and Bioengineering, Central South University, Changsha 410083, China

Abstract: The growing characteristics of metallic iron particles during reductive roasting of boron-bearing magnetite concentrate under different conditions were investigated. The size of the metallic iron particles was quantitatively measured via optical image analysis with consideration of size calibration and weighted ratio of image numbers in the core, middle and periphery zones of cross-section of pellets. In order to guarantee the measurement accuracy, 54 images were captured in total for each specimen, with a weighted ratio of 1:7:19 with respect to the core, middle and periphery section of the cross-section of pellets. Increasing reduction temperature and time is favorable to the growth of metallic iron particles. Based on the modification of particle size measurement, in terms of time (t) and temperature (T) a predicting model of metallic iron particle size (D), was established as: D=125−0.112t−0.2352T−5.355×10$^{-4}t^2$+2.032×10$^{-4}t\cdot T$+1.134×10$^{-4}T^2$.

Key words: ludwigite ore; reductive roasting; metallic iron; grain growth; size measurement

Cite this article as: ZHANG Xin, LI Guang-hui, RAO Ming-jun, MI Huan-peng, LIANG Bin-jun, YOU Jin-xiang, PENG Zhi-wei, JIANG Tao. Growth of metallic iron particles during reductive roasting of boron-bearing magnetite concentrate [J]. Journal of Central South University, 2020, 27(5): 1484−1494. DOI: https://doi.org/10.1007/s11771-020-4384-0.

1 Introduction

Ludwigite ore has not yet been utilized on an industrial scale because of its complex mineralogy and fine mineral dissemination as well as the low activity and grade of B_2O_3 [1]. Due to the increasing demand for boron and the depletion of szaibelyite ore of China, it is imperative to utilize ludwigite ore which accounts for about 58.54 wt.% boron resource [2]. At present, ludwigite ore was usually utilized via the process of magnetic-gravity separation, obtaining boron-bearing magnetite concentrate and boron concentrate [3, 4]. The boron concentrate can be used as the raw material for the production of borax or boric acid. While the boron-bearing magnetite concentrate needs further separation of boron and iron [5−7] .

The process of direct reduction followed by magnetic separation process is an effective way for the treatment of complex iron ores [8−11]. After direct reduction, the particle size of metallic iron plays an important role in this process because proper particle size is a key to achieving separation of iron by magnetic separation process, affecting the quality of the intermediate and final products. Based on the previous study, there are three main methods to measure the particle size, i.e., sieving, image analysis, and laser diffraction [12−17]. Many researchers have proved that the optical image

Foundation item: Project(51804346) supported by the National Natural Science Foundation of China; Project(2019JJ50767) supported by the Natural Science Foundation of Hunan Province, China; Project(KY [2017]125) supported by Youth Foundation of Guizhou Education Department, China
Received date: 2019-09-03; **Accepted date:** 2020-03-06
Corresponding author: RAO Ming-jun, PhD, Associate Professor; Tel: +86-18229897207; E-mail: mj.rao@csu.edu.cn; ORCID: 0000-0001-6032-9340

analysis was an effective way to measure the particle size of metallic iron [18, 19]. Thus, the method of image capture and the data analysis of particle size are the two key factors affecting the accuracy of the results in the measurement. On one hand, the growth of iron particles was simply carried out on the qualitative description; on the other hand, the quantitative description was very rough as it ignored two key factors of the measurement and evaluation of particle size, namely, weighted ratio and size calibration, especially in the research of metallic iron particle size during reductive roasting of boron-bearing magnetite concentrate.

In this paper, tests were carried out to investigate the effect of reduction temperature and time on the growth of metallic iron particles of boron-bearing magnetite concentrate. To get the insights into the characteristics of metallic iron particles, the volume frequency distribution and average size were quantitatively calculated based on weight and calibration during reductive roasting in 100 vol.% CO atmosphere. Based on these, the predicting model was set up to predict the average particle size of metallic iron in different reduction conditions of boron-bearing magnetite concentrate. Meanwhile, the growth mechanism on metallic iron particles was investigated. The results can provide a theoretical basis for the direct reduction of boron-bearing magnetite concentrate.

2 Materials and methods

2.1 Materials

The boron-bearing magnetite concentrate was taken from Liaoning Province of China. The sample was dried at 110 °C for 2 h, and then ground to 80 wt.% passing 74 μm. The chemical composition is shown in Table 1. The sample was characterized by low iron and boron contents. The contents of total iron and B_2O_3 were 52.11 wt.% and 5.25 wt.%, respectively. According to the XRD results, the concentrate mainly consists of magnetite (Fe_3O_4), szaibelyite ($Mg_2B_2O_4(OH)_2$), lizardite ($Mg_3Si_2O_5(OH)_4$) and magnesite ($MgCO_3$) [20−22].

CO (99.95 vol.% purity) and N_2 (99.999 vol.% high-purity) were used as the reducing and protective gases, respectively.

Table 1 Main chemical composition of boron-bearing magnetite concentrate (wt.%)

TFe	FeO	B_2O_3	SiO_2	Al_2O_3	CaO
52.11	24.65	5.25	5.36	0.39	0.62
MgO	K_2O	Na_2O	P	S	*LOI
12.61	0.05	0.17	0.014	1.15	2.45

*LOI is the mass loss on ignition.

2.2 Methods

2.2.1 Reduction roasting

Boron-bearing magnetite concentrate was ground to 80 wt.% passing 74 μm for pelletization. The green pellets with a diameter of 10−12 mm were dried at 110 °C for 2 h subsequently. The dry pellets were loaded into a quartz tube (inner diameter of 20 mm) which was introduced with N_2 in advance, and then the quartz tube was transferred into the furnace; the gas was shifted from N_2 to CO for reductive roasting when the furnace temperature was raised to the desired temperature (1000 °C, 1100 °C, 1200 °C). In all cases, the gas flow rate was fixed at 200 L/h. After roasting, the tube was taken out of the furnace to cool to room temperature with the protection of N_2 gas.

2.2.2 Particle size measurement

The reduced pellets were mounted with epoxy resin, and then cut, ground and polished to prepare cross-sections for microstructure observation. An optical microscope (LEICA DMI5000 M, Germany) was used to obtain microscopic images of metallic iron particles (magnification: 200 folds), and then the average size was measured by Image-Pro Plus 6.0 software.

Meanwhile, fracture surfaces of the pellets were also observed using environmental scanning electron microscopy (ESEM, FEI QUANTA 200, Holland) equipped in backscatter electron mode operating in a low vacuum of 66.6 Pa and 20 keV. The specimens were coated with gold prior to the detection. Spherical-like particles of metallic iron were commonly formed during reduction roasting (Figure 1(a)). Metallic iron particles are inerratic spherical shape in the three- dimensional space, so the projection could be regarded as being two-dimensionally round. Then, the particle size can be calculated according to Eq. (1).

$$L=\sqrt{\frac{4A}{\pi}} \tag{1}$$

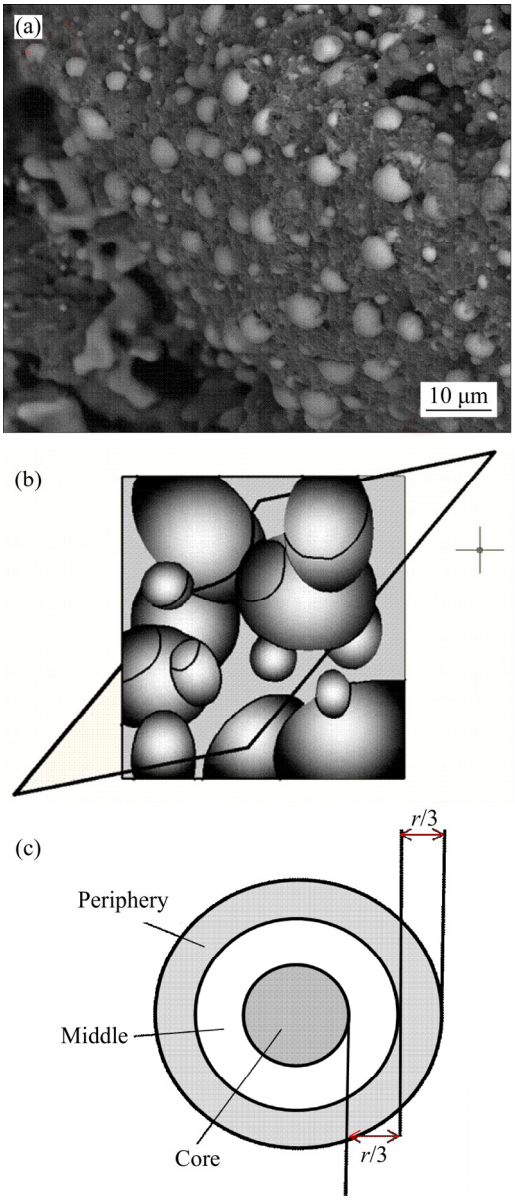

Figure 1 BSE microphotograph of metallic iron particles in reduced pellet (1100 °C, 60 min) (a), random cutting through spherical particles (b) and division of periphery, middle and core in a pellet (c)

where L is the two-dimensional diameter; A is the cumulative area of metallic iron particles.

Nevertheless, the cutting surface might not go through the center of particles. Therefore, the vast majority of cross sections in the two-dimensional space are not the true diametrical sections of particles, as shown in Figure 1(b). Therefore, the true particle size (D) should be modified by Eq. (2) [23, 24].

$$D=\frac{4L}{\pi}=\frac{4\sqrt{\frac{4A}{\pi}}}{\pi}=\frac{8\sqrt{A}}{\pi\sqrt{\pi}} \tag{2}$$

In reduction process, the pellets structure and the diffusion of reducing gas, etc will affect the reduction degree through the pellet diameter, and the number of the microscopic images should be selected according to a certain weighted ratio. Firstly, as shown in Figure 1(c), three zones (periphery, middle and core) were divided across the cross-section of reduced pellets. Then microscopic images were recorded and saved in the computer according to a certain weight ratio in each zone.

Assuming that the weighed ratio of optical image numbers in the core, middle and periphery zones was a: b: c, to obtain additional details, the boron-bearing magnetite concentrate pellet was reduced at 1100 °C for 10 min and the reduced sample after polished was taken into evaluation. Determination of the weighted ratio (a: b: c) was based on Eq. (3) [25].

$$\frac{RT}{M}\ln\left(\frac{c_1}{c_2}\right)=\frac{2\sigma}{\rho}\left(\frac{1}{r_1}-\frac{1}{r_2}\right) \tag{3}$$

where M is molar mass; c_i (i=1, 2) is the concentration of particles; r_i (i=1, 2) is the curvature radius of particles; σ is surfacetension; ρ is density.

By transforming Eq. (3), then we get:

$$\ln c_1-\ln c_2\propto\frac{1}{r_1}-\frac{1}{r_2} \tag{4}$$

The relationship of concentration and curvature radius of particles could be obtained:

$$\ln c\propto\frac{1}{r} \tag{5}$$

According to the different principles (time ratio, ratio of time evolution, linear ratio, area ratio and volume ratio), the least square method was used for the linear regression fitting. The fitting results of different weighted ratio were obtained.

Based on this, the actual image numbers of the core, middle and periphery zones were set as 2, 14 and 38, respectively. 54 images were taken in total for each specimen. The measurement method then is able to quantitatively describe the particle size of metallic iron, providing theoretical guidance for the measurement of particle size.

2.2.3 Evaluation index

The particle size characterization is often expressed as the distribution of volume frequency and cumulative frequency. In this study, the frequency distribution of metallic iron particles was

calculated using the following equations.

1) Volume frequency distribution ($V(D)$):

$$V_r(D_i)=\frac{D_i^2\times n_i}{\sum_{i=1}^{N}\left(D_i^3\times n_i\right)} \tag{6}$$

where D_i is the true particle size; n_i is the number of particles; N is the total number of particles.

2) Cumulative frequency distribution ($Q(D)$):

$$Q(D_i)=\frac{\sum_{i=1}^{i} n_i}{\sum_{i=1}^{N} n_i} \tag{7}$$

3) Average size: The diameter corresponding to the cumulative size distribution ratio of 50% (D_{50}) was defined as the apparent average size of metallic iron particles.

3 Results and discussion

3.1 Morphologies

The pellets reduced for 60 min at different temperatures were fractured for cross-section observation by SEM (Figure 2).

Metallic iron particles at 1000 °C were tiny and deformed. At the temperature of 1100 °C, metallic iron particles began to emerge and aggregate obviously; however, the appearance of the metallic iron was dim and attached impurities. While at 1200 °C, metallic iron particles with larger size and less impurity were precipitated from the basal body. The appearance of the metallic iron particles was smooth and bright.

By correlating the growth of metallic iron particles with the morphologies well discriminated by the SEM analysis, it may be noted that the temperature increase was responsible for the growth of metallic iron particles with the same reduction time. The metallic iron particles size increased with the rising of reduction temperature.

The SEM images of boron-bearing magnetite concentrate ore pellets reduced for different times at temperature of 1200 °C are recorded as presented in Figure 3. At the early stage of the reduction process (about 5 min, Figure 3(a)), the reaction between iron oxides and CO occurred. Thus, a few metallic iron particles with very fine sizes were produced and located at the surface of mineral particles. After reduction for 10 min (Figure 3(b)), the metallic iron particles separated from the basal body and contacted with each other gradually, and forwarded into the center of mineral particles.

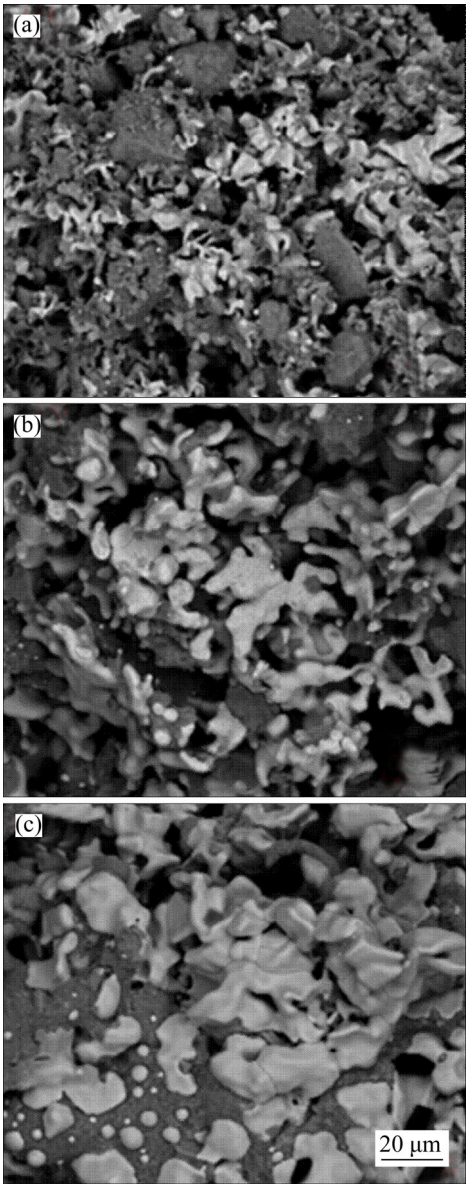

Figure 2 Morphology of boron-bearing magnetite concentrate pellets reduced for 60 min at different temperatures: (a) 1000 °C; (b) 1100 °C; (c) 1200 °C

Both the amount and particle size of the metallic iron increased with a prolonged reduction time of 30 min, as shown in Figure 3(c). When the reduction time was prolonged further, to 45 min or longer, the connection between the metallic iron particles with larger size occurred, which accounts for polygonization and densification. Therefore, the reduction time played an important role in the growth of metallic iron particles. The metallic iron particles size increased with the prolonging of reduction time.

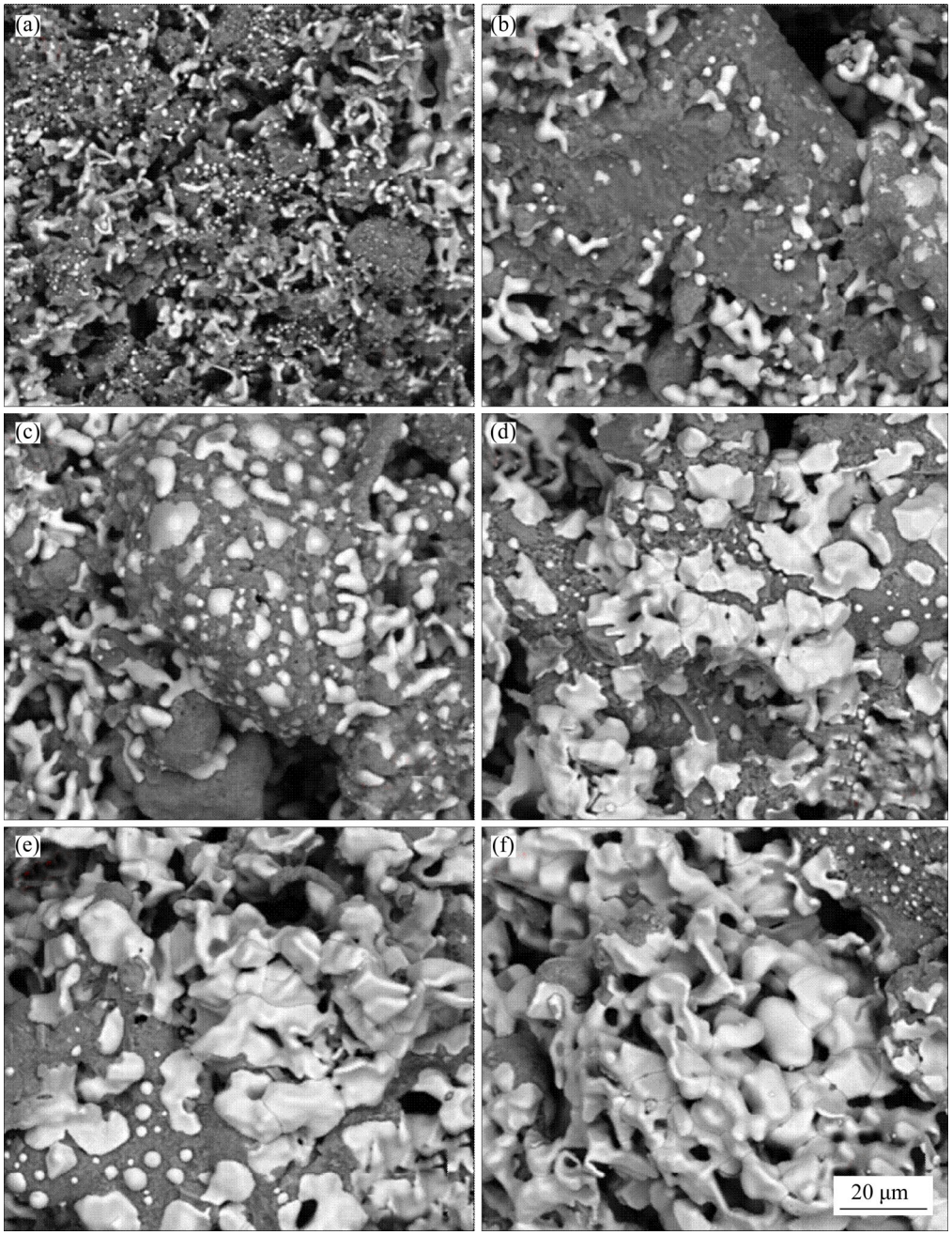

Figure 3 Morphology of reduced boron-bearing magnetite concentrate pellets after reduction at 1200 °C for different time: (a) 5 min; (b) 15 min; (c) 30 min; (d) 45min; (e) 60 min; (f) 90 min

3.2 Volume frequency distribution

During the reduction process, the massive micro-grade metallic iron particles will reduce the average particle size, while the main evaluation standards of dissociation depend on the proportion of large particle size. To investigate the effect of reduction temperature and time on the volume frequency distribution, several comparative tests were carried out under different reduction conditions. The results are shown in Figure 4.

It can be seen from Figure 4 that the metallic iron particle distribution interval and the proportion of large particle size both increased with the increase of reduction temperature and reaction time. For example, in Figure 4(a), at a constant roasting temperature of 1000 °C, when the roasting time was 5 min, the metallic iron particle distribution interval was only 0−60 μm, and the proportion of 60 μm was only 0.60 wt.%. As the reaction time elongated to 90 min, the interval extended to 0−125 μm, and the proportion of 125 μm was 3.19 wt.%. Furthermore, it is evident that with a fixed roasting

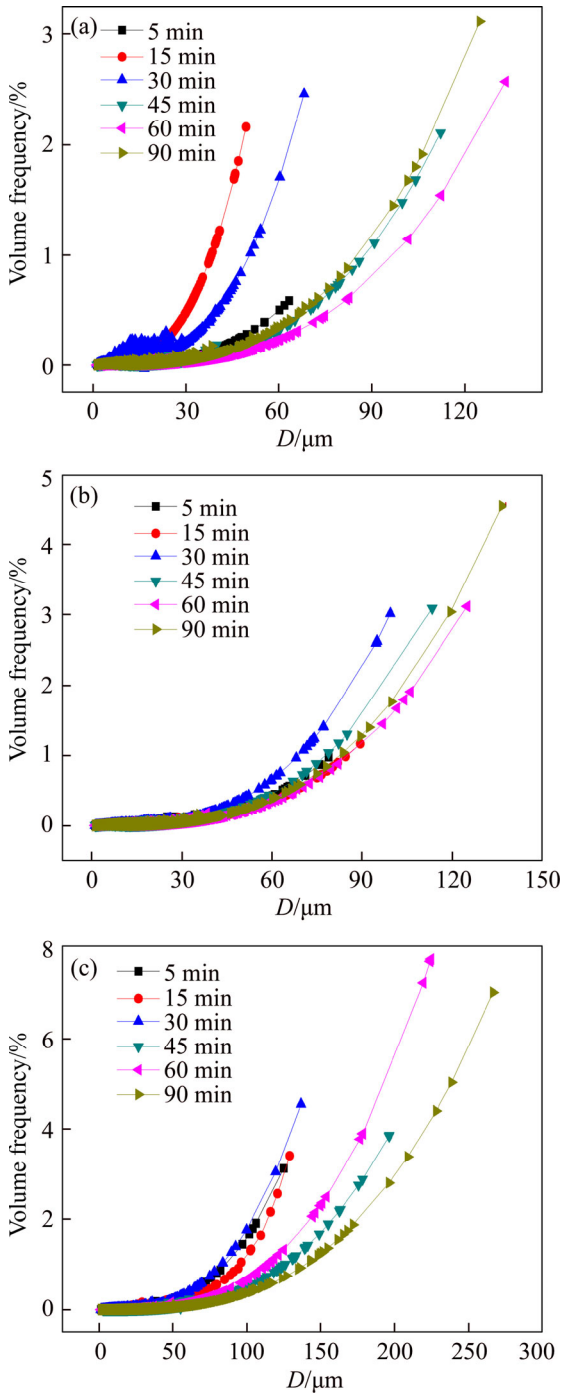

Figure 4 Volume frequency distribution of metallic iron particles after reduction for 60 min at different temperatures: (a)1000 °C; (b) 1100 °C; (c) 1200 °C

period of 60 min, when the reduction temperature was 1000, 1100 and 1200 °C, the metallic iron particle distribution interval was 0−124 μm, 0−133 μm and 0−224 μm, and the proportion of the largest particle size was 2.57 wt.%, 3.12 wt.% and 7.74 wt.%, respectively.

The extension of metallic iron particle distribution interval was favorable to the improvement of iron recovery and metallization, and therefore, improved the efficiency of subsequent magnetic separation.

3.3 Cumulative frequency distribution and average size (D_{50})

The cumulative frequency distribution of metallic iron particles in the reduced samples is shown in Figure 5. With the extension of reduction

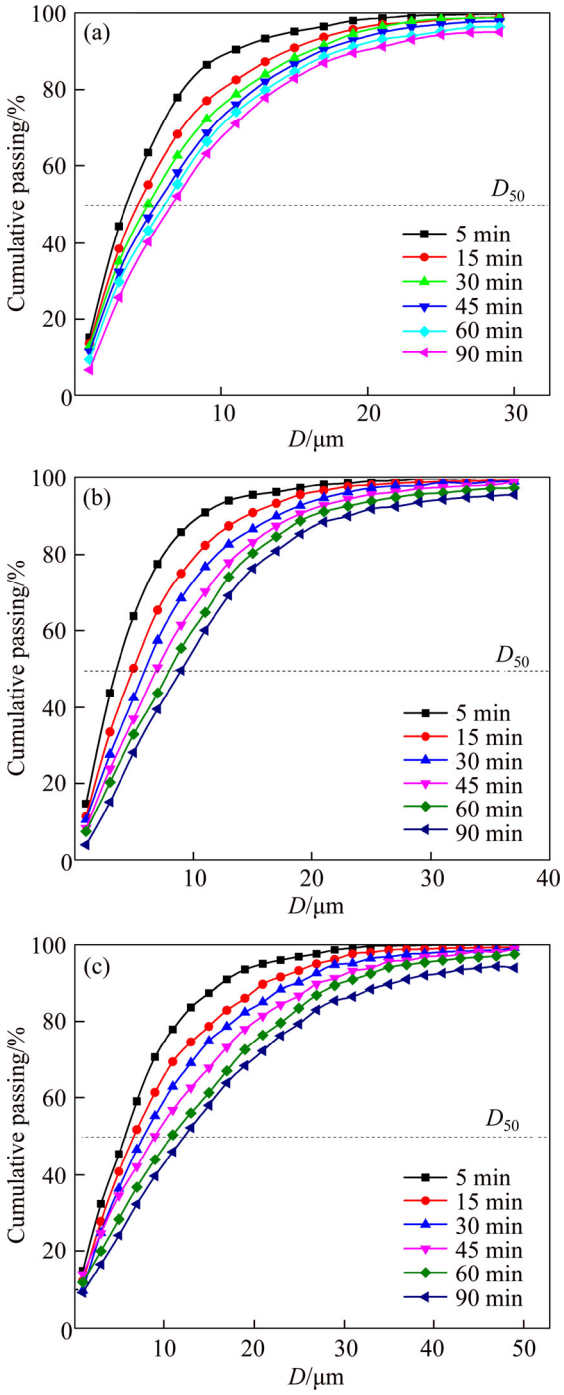

Figure 5 Cumulative size distribution of metallic iron particles of pellets reduced at different temperatures: (a) 1000 °C; (b) 1100 °C; (c) 1200 °C

time, the cumulative frequency distribution curve of metallic iron particles moved to the bottom right in turn, indicating that the proportion of micro-grade metallic iron particles decreased gradually with the extension of reduction time. Likewise, the curves shift to the right successively with rising reduction temperature for the same reduction time, illustrating that the number of large metallic iron particles increases. These phenomena were attributed to the fact that the increase of reduction time and temperature could accelerate the growth of metallic iron particles, and more large particles were formed under higher temperatures or longer reduction time [26].

The average sizes of metallic iron particles under different reduction conditions are shown in Figure 6. It can be seen that rising reduction temperature and prolonging reaction time are both beneficial for the average size of metallic iron particles. The metallic iron particles size increased from 4.38 to 9.06 μm with reduction time prolonging from 5 min to 90 min at 1100 °C; likewise, the average size increased from 6.22 to 11.51 μm with reduction temperature rising from 1000 °C to 1200 °C for 45 min.

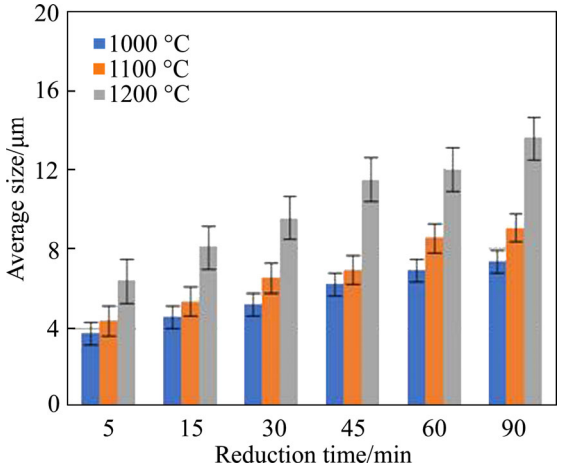

Figure 6 Average size of metallic iron particles in reduced pellets

3.4 Predicting model

The predicting model between metallic iron particle size and reduction temperature as well as reduction time was established. With reduction temperature T (°C) and reduction time t (min) as the independent variables, average particle size D (μm) of metallic iron as dependent variables, four models were set up. According to the experimental data in Figure 6, the least squares regression analysis was chosen via MATLAB software, and the fitting results are shown in Table 2 and Figure 7.

Table 2 Fitting results of different models

Model	Fitting equation	Correlation coefficient, R^2
1	$f(t, T)=a_0+a_1t+a_2T$ $D=-19.84+0.06096t+0.02264T$	0.8838
2	$f(t, T)=a_0+a_1t+a_2T+a_3tT+a_4T^2$ $D=125.8-0.1625t-0.2352T+2.032\times10^{-4}tT+1.34\times10^{-4}T^2$	0.9588
3	$f(t, T)=a_0+a_1t+a_2T+a_3t^2+a_4tT$ $D=-11.45-0.112t+0.01435T-5.355\times10^{-4}t^2+2.032\times10^{-4}tT$	0.9359
4	$f(t, T)=a_0+a_1t+a_2T+a_3t^2+a_4tT+a_5T^2$ $D=125-0.112t-0.2352T-5.355\times10^{-4}t^2+2.032\times10^{-4}tT+1.134\times10^{-4}T^2$	0.9870

The fitting result of Model 4 was the best with correlation coefficient reaching to 0.9870. Therefore, the established predicting equation of Model 4 can be used to evaluate the average particle size of metallic iron in different reduction conditions. Thus, the equation of particle size of metallic iron can be expressed as: $D=125-0.112t-0.2352T-5.355\times10^{-4}t^2+2.032\times10^{-4}tT+1.134\times10^{-4}T^2$.

4 Conclusions

1) The size calibration and weighted ratio of image numbers in the core, middle and periphery zones of cross-section of pellets were taken into consideration for the particle size measurement of metallic iron. The fitting results of different weighted ratio of image numbers in different zones of cross-section showed that weighted ratio of 1:7:19, with respect to the core, middle and periphery section, got the highest correlation coefficient. In order to guarantee the measurement accuracy, 54 images were captured in total for each specimen.

2) The volume frequency distribution and average size were quantitatively determined. Raising reduction temperature and prolonging reaction time were both beneficial for the growth of metallic iron particle. The predicting model of average particle size D_{50} (μm) with respect to reduction temperature T (°C) and reduction time t (min) was established as: $D=125-0.1125t-0.2352T-5.355\times10^{-4}t^2+2.032\times10^{-4}tT+1.134\times10^{-4}T^2$.

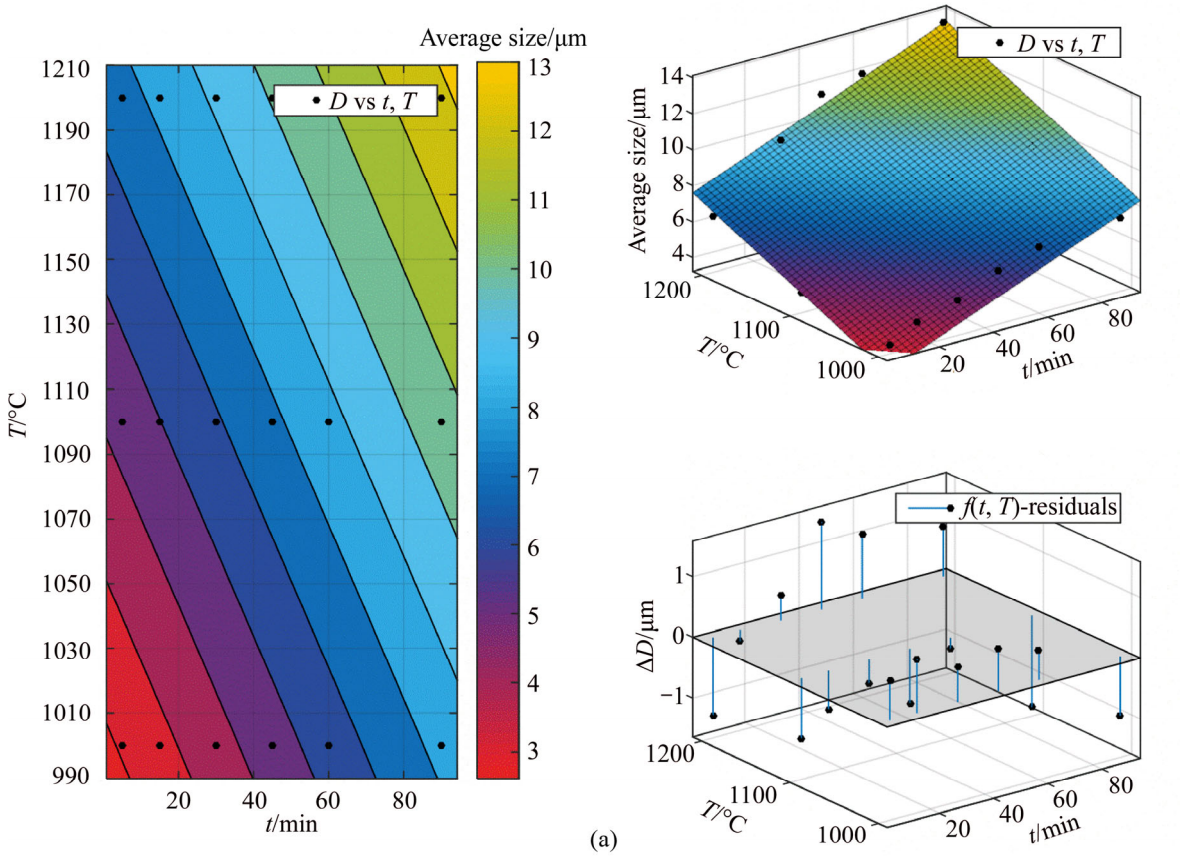

(a)

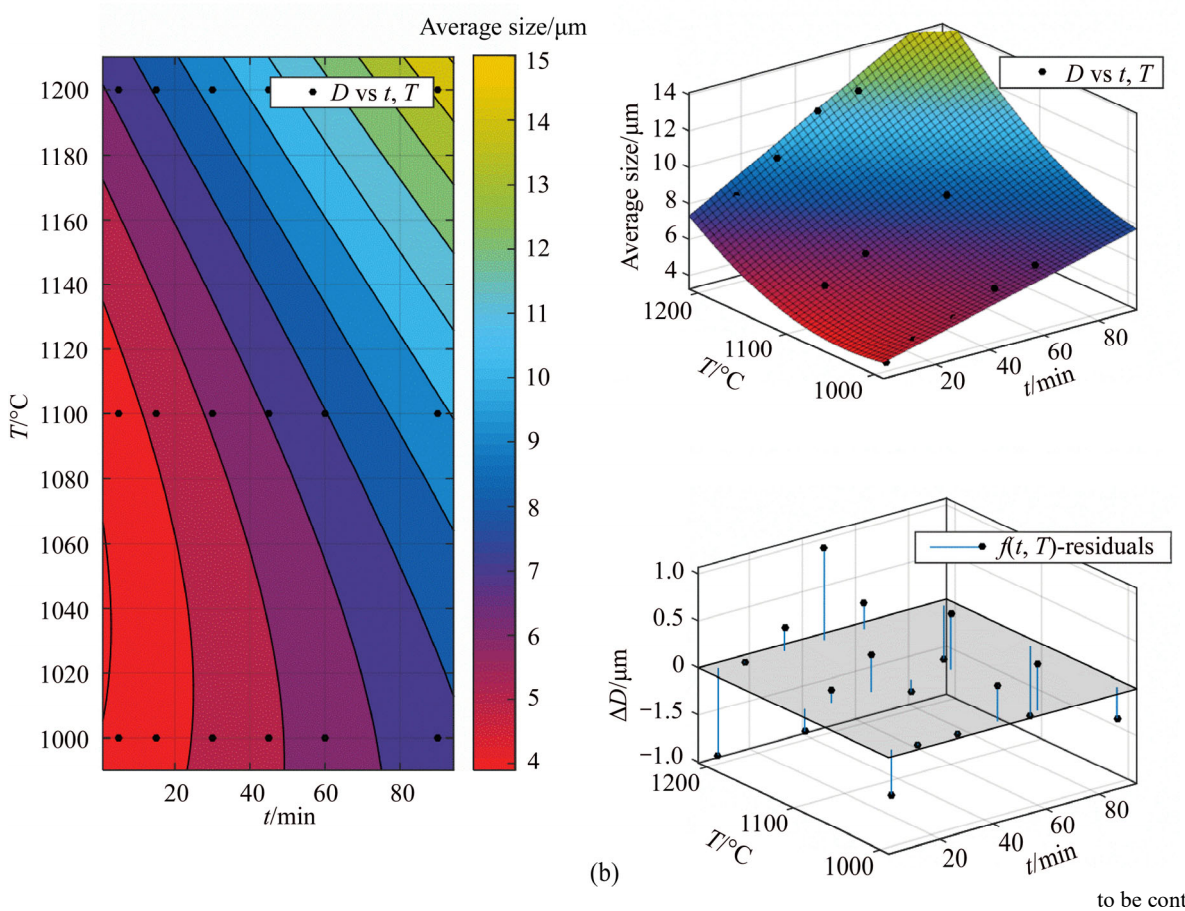

(b)

to be continued

continued

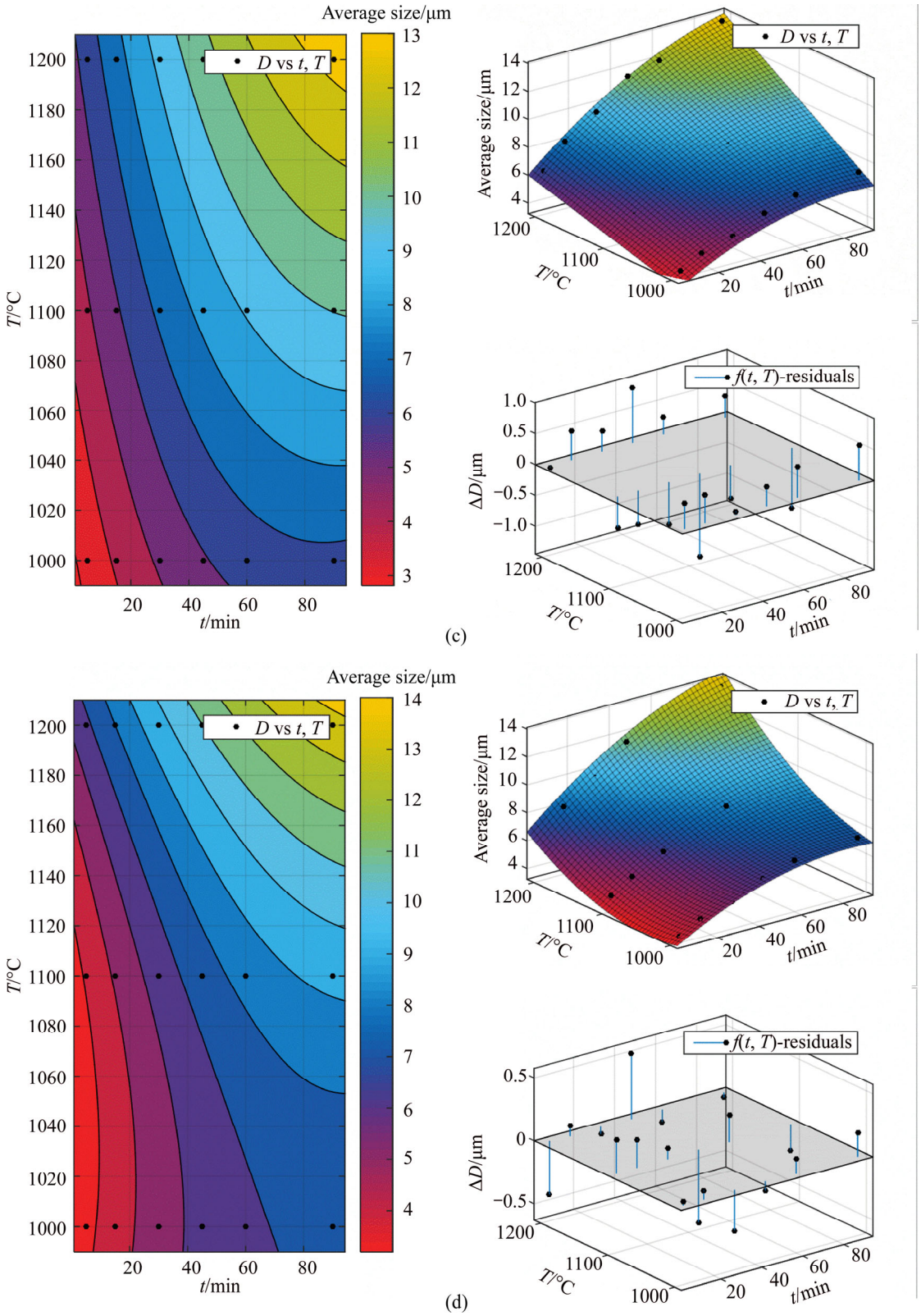

Figure 7 Fitting results of different models: (a) Model 1; (b) Model 2; (c) Model 3; (d) Model 4

References

[1] GAO P, YU J W, HAN Y X, ZHOU M G. Mineralogical study of boron-bearing iron concentrate ore [J]. Journal of Northeastern University, 2015, 36(4): 581−584. DOI: 10.3969 /j.issn.1005-3026. 2015.04. 027. (in Chinese)

[2] LIU R, XUE X X, LIU X, WANG D S, FENG C, HUANG D

W. Progress on China's boron resource and the current situation of boron-bearing materials [J]. Bulletin of the Chinese Ceramic Society, 2006, 25(6): 102−107. DOI: 10.16552/ j.cnki.issn1001-1625.2006.06.025. (in Chinese)

[3] ZHAO Q J, WANG C R, WANG C R, LIAN X Q. New process of multipurpose utilization of ludwigte [J]. Journal of Northeastern University (Natural Science), 1996, 17(6): 588−592. DOI: http://www.cnki.com.cn/Article/CJFDTotal-DBDX606.002.htm. (in Chinese)

[4] CAO Z, CAO Y D, GUI F. Research status and progress of the exploitation and utilization of Paigeite ore [J]. Multipurpose Utilization of Mineral Resources, 2013(2): 17−20. DOI:10.3969 /j.issn.1000-6532.2013.02.005. (in Chinese)

[5] WANG G, XUE Q G, WANG J S. Carbothermic reduction characteristics of ludwigite and boron-iron magnetic separation [J]. International Journal of Minerals Metallurgy and Materials, 2018, 25(9): 1000−1009. DOI: 10.1007/ s12613-018-1650-3.

[6] WANG Guang, WANG Jing-song, XUE Qing-guo. Properties of boron-rich slag separated from boron-bearing iron concentrate [J]. Journal of Central South University, 2018, 25: 783−794. DOI: 10.1007/s11771-018-3783-y.

[7] ZHANG X, LI G H, YOU J X, WANG J, LUO J, DUAN J, ZHANG T, PENG Z W, RAO M J, JIANG T. Extraction of boron from ludwigite ore: Mechanism on soda-ash roasting of Lizardite and Szaibelyite [J]. Minerals, 2019, 9(9): 533. DOI: https://doi.org/10.3390/min9090533.

[8] LIU G S, STREZOV V, LUCAS J A, WIBBERLEY L J. Thermal investigations of direct iron ore reduction with coal [J]. Thermochimica Acta, 2004, 410(1, 2): 133−140. DOI: 10.1016/s0040-6031(03)00398-8.

[9] PARISI D R, LABORDE M A. Modeling of counter current moving bed gas-solid reactor used in direct reduction of iron ore [J]. Chemical Engineering Journal, 2004, 104(1−3): 35−43. DOI: 10.1016/j.cej.2004.08.001.

[10] RAO M, LI G, ZHANG X, LUO J, PENG Z, JIANG T. Reductive roasting of nickel laterite ore with sodium sulfate for Fe-Ni production. Part I: Reduction/sulfidation characteristics [J]. Separation Science and Technology, 2016, 51(8): 1408−1420. DOI:10.1080/01496395.2016.1162173.

[11] LI G, YOU Z, ZHANG Y, RAO M, WEN P, GUO Y, JIANG T. Synchronous volatilization of Sn, Zn, and As, and preparation of direct reduction iron (DRI) from a complex iron concentrate via CO reduction [J]. JOM Journal of the Minerals Metals and Materials Society, 2014, 66(9): 1701−1710. DOI: 10.1007/s11837-013-0852-4.

[12] AL-THYABAT S, MILES N J. An improved estimation of size distribution from particle profile measurements [J]. Powder Technology, 2006, 166(3): 152−160. DOI: 10.1016/ j.powtec.2006.05.008.

[13] DONSKOI E, SUTHERS S P, FRADD S B, YOUNG J M, CAMPBELL J J, RAYNLYN T D, CLOUT J M F. Utilization of optical image analysis and automatic texture classification for iron ore particle characterisation [J]. Minerals Engineering, 2007, 20(5): 461−471. DOI: 10.1016/ j.mineng.2006.12.005.

[14] HUKKANEN E J, BRAATZ R D. Measurement of particle size distribution in suspension polymerization using in situ laser backscattering [J]. Sensors and Actuators B-Chemical, 2003, 96(1, 2): 451−459. DOI: 10.1016/s0925-4005(03) 00600-2.

[15] KOH T K, MILES N J, MORGAN S P, HAYES-GILL B R. Improving particle size measurement using multi-flash imaging [J]. Minerals Engineering, 2009, 22(6): 537−543. DOI: 10.1016/j.mineng.2008.12.005.

[16] SUN Y, HAN Y, GAO P, YU J. Size distribution behavior of metallic iron particles in coal-based reduction products of an oolitic iron ore [J]. Mineral Processing and Extractive Metallurgy Review, 2015, 36(4): 249−257. DOI: 10.1080/ 08827508.2014.955611.

[17] MAITI A, CHAKRAVARTY D, BISWAS K, HALDER A. Development of a mass model in estimating weight-wise particle size distribution using digital image processing [J]. International Journal of Mining Science and Technology, 2017, 27(3): 435−443. DOI: 10.1016/j.ijmst.2017.03.015.

[18] DONSKOI E, RAYNLYN T D, POLIAKOV A. Image analysis estimation of iron ore particle segregation in epoxy blocks [J]. Minerals Engineering, 2018, 120: 102−109. DOI: 10.1016/j.mineng.2018.02.024.

[19] LUO L, ZHANG H. Process mineralogy and characteristic associations of iron and phosphorus-based minerals on oolitic hematite [J]. Journal of Central South University, 2017, 24(9): 1959−1967. DOI:10.1007/s11771-017-3604-8.

[20] LI G, LIANG B, RAO M, ZHANG Y, JIANG T. An innovative process for extracting boron and simultaneous recovering metallic iron from ludwigite ore [J]. Minerals Engineering, 2014, 56: 57−60. DOI: 10.1016/j.mineng. 2013.10.030.

[21] LIANG B, LI G, RAO M, PENG Z, ZHANG Y, JIANG T. Water leaching of boron from soda-ash-activated ludwigite ore [J]. Hydrometallurgy, 2017, 167: 101−106. DOI: 10.1016/j.hydromet.2016.11.004.

[22] LI G, FANG L, ZHANG X, LIANG B, RAO M, PENG Z, JIANG T. Utilization of the MgO-rich residue originated from Ludwigite ore: Hydrothermal synthesis of MHSH whiskers [J]. Minerals, 2017, 7(8): 138−145. DOI: 10.3390/ min7080138.

[23] CHAYES F. On the bias of grain-size measurements made in thin section [J]. Journal of Geology, 1950, 58(2): 156−160. DOI: 10.1086/625716.

[24] CUZZI J N, OLSON D M. Recovering 3D particle size distributions from 2D sections [J]. Meteoritics & Planetary Science, 2016, 52(3): 532−545. DOI:10.1111/maps.12812.

[25] NAPPER D H. Particle growth in suspensions [J]. Journal of Colloid & Interface Science, 1974, 46(1): DOI: 10.1016/ 0021-9797(74)90040-X.

[26] SUN Y S, HAN Y X, LI Y F, LI Y J. Formation and characterization of metallic iron grains in coal-based reduction of oolitic iron ore [J]. International Journal of Minerals Metallurgy & Materials, 2017, 24(2): 123−129. DOI: 10.1007/s12613-017-1386-5.

(Edited by YANG Hua)

中文导读

含硼铁精矿还原焙烧过程中金属铁颗粒的生长规律

摘要：研究了不同还原条件下含硼铁精矿在焙烧过程中金属铁颗粒的生长规律。采用光学显微镜获取还原球团的数字图像，考虑到球团不同部位金属铁颗粒生长情况的差异，采用回归拟合分析得到内、中、外区域的权重比例为 1:7:19，每个样品根据此权重比例共获取 54 张图像。基于修正后的金属铁颗粒尺寸的测定方法，建立了铁颗粒平均粒径 D (μm)与还原温度 T (°C)、时间 t (min)之间的回归模型：$D=125-0.112t-0.2352T-5.355\times10^{-4}t^2+2.032\times10^{-4}tT+1.134\times10^{-4}T^2$。

关键词：硼铁矿；还原焙烧；金属铁；颗粒生长；粒径测定